BMC Genomics

RESEARCH

Open Access

Integrated multiomic profiling of tail adipose tissue highlights novel genes, lipids, and metabolites involved in tail fat deposition in sheep

Yujing Xie[1†], Xin Li[1†], Huili Liang[1], Mingxing Chu[2], Guiling Cao[1,3*] and Yunliang Jiang[3*]

Abstract

Background Tail fat is important for fat-tailed or fat-rumped sheep to survive in harsh environments. However, the molecular mechanism underlying tail fat deposition in sheep remains unclear. In this study, we comprehensively characterized the transcriptome, untargeted lipidome, and targeted metabolome profiles of the tail adipose tissues from Large-tailed Han sheep (long fat-tailed sheep) and Hu sheep (short fat-tailed sheep).

Results We identified 183 differentially expressed genes (DEGs), 55 differential lipids (DLs) and 17 differential metabolites (DMs) in the adipose tissues of the tails from Large-tailed Han and Hu sheep. Among the 183 DEGs selected (Q values ≤ 0.05 and $|\log_2(FC)| \geq 0.5$), 18 DEGs, such as *UCP3*, *ELOVL7* and *GDF10*, were directly associated with lipid metabolism identified via Gene Ontology (GO) analysis. Some genes, such as *PPP3R1A*, *ADRA1*, and *DSLC46A2*, were reportedly associated with lipid metabolism. A fold change ≥ 1.2 or ≤ 0.83 and a P-value < 0.05 were set as the default threshold to select the DLs and DMs. Among the 55 DLs, 36 DLs were phosphatidylcholines and 9 DLs were phosphatidylethanolamines. The top six DLs with the greatest differences in content were LPE (20:4) (up), PC (42:10) (up), PC (42:8) (up), PC (16:1/16:1) (down), PC (29:0) (down), and PC (32:2) (down). DMs related to the tricarboxylic acid cycle, such as D-glucose, cis-aconitic acid and citric acid were abundant in the tail fat of Large-tailed Han sheep. The DEGs, DLs and DMs were enriched mainly in the ferroptosis, the extracellular matrix (ECM)-receptor interaction, cGMP-PKG, calcium signaling and pathways related to cardiomyopathy and the tricarboxylic acid cycle.

Conclusion This study obtained profiles of the transcriptome, lipidome and metabolome of the tail fat tissues of sheep with long and short fat tails. The findings suggested that *ELOVL7*, *UCP3* and ferroptosis, ECM-receptor interaction pathways contributed to the difference in fat deposition, and phosphatidylcholines biosynthesis and tricarboxylic acid cycle may affect lipid metabolism in sheep tails. The results enhance our understanding of the differences in fat deposition in sheep tail.

[†]Yujing Xie and Xin Li contributed equally to this work.

*Correspondence:
Guiling Cao
cglling@126.com
Yunliang Jiang
zhaojy@sdau.edu.cn

Full list of author information is available at the end of the article

Keywords Sheep, Tail adipose tissues, Transcriptome, Lipidome, Metabolome

Introduction

Tail fat is essential for the survival of fat-tailed or fat-rumped sheep in cold and drought environments [1, 2]; additionally, it can serve as a high-energy food source for humans during periods of drought and famine [3]. However, in recent years, sheep tail fat has no longer been favored by consumers because of changes in dietary habits. Additionally, in modern livestock production systems, the presence of a long fat tail in sheep presents several disadvantages, such as being unfavorable for mating [4]. Consequently, intensive production and changes in commercial demand have led to a reduction in genetic diversity in local sheep varieties [5]. The population of long fat-tailed sheep has consequently diminished. The conservation of long fat-tailed sheep populations is crucial for the future of sheep breeding, the protection of genetic diversity and the ability to respond to unpredictable climate change [6]. Understanding the mechanisms underlying tail fat deposition will be instrumental in conservation efforts for these sheep. Recently, some studies have focused on searching for major genes related to the tail types of sheep via genome-wide association studies, the detection of selective sweeps and transcriptome analysis. Some genes, such as *PDGFD* [7, 8], *BMP2* [7, 9], *PPP2CA* and some LncRNAs (e.g., MSTRG.24995 and MSTRG.36913) [10, 11] are associated with the tail phenotype of sheep. Some biological processes, such as extracellular matrix (ECM) remodeling, lipid metabolism and terminal adipogenic differentiation [8, 12], are involved in tail fat deposition in sheep.

The Large-tailed Han (LTH) sheep is a well-known long fat-tailed sheep breed in China. The fat tail of this sheep is long, large, and fan shaped and hangs down to the hocks. The tail fat weight of six-month-old male LTH sheep accounts for approximately 16% of the total body weight [13]. Hu sheep are short fat-tailed sheep (Fig. 1) and their tail fat weight accounts for 3% of their body weight [14]. The two sheep breeds with distinct tail phenotypes provide materials for elucidating the mechanisms related to fat deposition in and the length of the tail. In addition, the large amount of fat deposited in tails of LTH sheep does not cause metabolic disorders. Currently, obesity and associated metabolic syndrome caused by increased fat deposition are challenging public issues and economic burdens [15]. The mechanism of fat distribution in the sheep tail may provide some unconventional ideas for preventing metabolic diseases related to obesity in humans. Here, we compared the transcripts, lipids and metabolites of tail adipose tissues from LTH and Hu sheep and aimed to identify new genes and signaling pathways that contribute to the differences in tail fat distribution in sheep. The differences in lipid composition and metabolites may provide new ideas for the utilization of sheep tail fat.

Materials and methods

Animals and adipose tissue collection

The animal experiment was carried out in Liaocheng city (36°N, 116°E), Shandong Province, China. Six clinically normal one-year-old male LTH sheep (body weight (BW), 52.61 ± 2.08 kg) and six one-year-old Hu sheep (BW, 48.80 ± 3.27 kg) fed with the same total mixed ration diet were sacrificed in the summer (July 2023) after anesthesia by injecting pentobarbital sodium (30 mg/kg BW; Ningbo, China) through the ear vein. The adipose tissues from the tails of LTH and Hu sheep were collected and stored in liquid nitrogen until further processing. For convenience, throughout the remainder of the manuscript, the adipose tissue from the tails of LTH and Hu sheep is referred to as LTF (Large-tailed Han sheep tail fat) and HTF (Hu sheep tail fat), respectively.

RNA-seq of tail adipose tissue

RNA extraction and sequencing

Total RNA from tail adipose tissues was extracted using a TRIzol-based method. The purity, concentration and integrity of extracted RNA from each sample were checked using an Agilent Fragment Analyzer (Agilent, Germany) and agarose gel electrophoresis. Because of poor quality, the total RNA extracted from the adipose tissue of two LTH sheep was not suitable for RNA-seq; therefore, RNA from four LTH sheep and four Hu sheep was subjected to RNA sequencing. RNA was denatured at a suitable temperature, and poly(A)-RNA was enriched using oligo (dT)-attached magnetic beads. After fragmentation, the poly(A)-RNA was used to synthesize double-stranded cDNA (dscDNA). The synthesized dscDNA was subjected to an end repair reaction. Then, a single 'A' nucleotide was added to the 3' end of dscDNA fragments through an A tailing reaction and followed by ligation with adapters. dscDNAs ligated with adapters were amplified via PCR. Next, through dscDNA denaturation, single-stranded PCR products were produced and ligated to obtain single-stranded cyclized DNA products. Using the rolling cycle amplification method, a DNA nanoball containing multiple copies of single-stranded circularized DNA was produced. Then, the DNA nanoballs were evaluated for quality and sequenced on the DNBSEQ platform (BGI, China).

Fig. 1 Chinese indigenous sheep breeds with different tail types. **A**, Large-tailed Han sheep. **B**, Hu sheep. The photo of Hu sheep was from the website of the National germplasm center of domestic animal resources, China

Differentially expressed genes (DEGs) identification

Raw RNA-seq reads were first filtered using SOAPnuke (v1.5.6) [16] to obtain clean reads, which were then mapped to the reference genome (*Ovis aries*, GCF_000298735.2_Oar_v4.0) using HISAT2 (v2.1.0) and to the gene set using Bowtie 2 (v2.3.4.3) [17, 18]. Gene expression quantification was performed using RSEM (v1.3.1) [19]. DESeq2 (v1.4.5) was used to conduct differential expression analysis [20]. Heatmaps were drawn using pheatmap (v1.0.8) according to the differences in gene expression among different samples. On the basis of the normalized gene expression level, the fold change (FC) values were estimated, and the *Q* values were modified according to *P* values. The default thresholds to identify DEGs were *Q* value ≤ 0.05 and $\left| \mathrm{Log}_2(\mathrm{FC}) \right| \geq 0.5$ [21].

Functional enrichment analyses of DEGs

Gene Ontology (GO) (http://www.geneontology.org/) and Kyoto Encyclopedia of Genes and Genomes (KEGG) (https://www.kegg.jp/kegg/) enrichment analyses were performed to annotate the functions of the DEGs via Phyper using a hypergeometric test. *P* value < 0.05 was set as the threshold to define the significant enrichment of GO or KEGG terms. A protein-protein interaction network was constructed using the STRING database schema v12.0 (organism, Ovis aries).

Validation of mRNA by RT–qPCR

cDNA was generated from total RNA using a PrimerScript™ RT Kit (Takara, China). Reverse transcription quantitative real-time PCR (RT–qPCR) was performed on an Applied Biosystems (ABI) CFX96 Touch Real Time Detection System using SYBR Green qPCR Master Mix (Thermo Fisher, America) for six genes with designed primers (Table S1). *ACTB* was used as a reference gene, and the $2^{-\Delta\Delta Ct}$ method was used to measure the relative expression levels. Statistical analysis was performed via *t* tests.

Untargeted lipidomics of tail adipose tissue

Metabolite extraction

A total of 25 mg of adipose tissue from each sample was homogenized in 800 μL of precipitant (prechilled methanol/dichloromethane (1:3, v/v, 10 μL of internal standard added) for 5 min, ultrasonically treated for 10 min in an ice bath and then incubated overnight at -20 ℃. After centrifugation, 600 μL of the supernatant was extracted, freeze-dried, and then dissolved in 600 μL of a lipid reconstitution solution (isopropanol: acetonitrile: water = 2:1:1) for 10 min, followed by ultrasonication (ice bath) for 10 min and centrifugation at 25,000×g at 4 ℃ for 15 min. A total of 10 μL of the supernatant was mixed with a quality control sample for subsequent liquid chromatography–tandem mass spectrometry (LC–MS/MS) analysis.

LC–MS method for lipid analysis

An ultra-performance liquid chromatography (UPLC) I-Class Plus (Waters, USA) tandem Q Exactive mass spectrometer (Thermo Fisher) was used to separate and detect lipids which was conducted by BGI Biotech, according to the protocol previously described by Chang [22]. The chromatographic conditions were as follow: CSH C18 column (1.7 μm, 2.1 mm ×100 mm, Waters); negative ion mode with mobile phase A: 60% acetonitrile-water + 10 mmol/L ammonium formate and phase B: acetonitrile/isopropanol (1/9, V/V) + 10 mmol/L ammonium formate; and 0.1% formic acid was added to phases A and B for negative ion mode to form phase A and B for positive ion mode. The gradient conditions were as follows: 0–2 min, 40–43% B; 2–2.1 min, 43–50% B; 2.1–7 min, 50–54% B; 7–7.1 min, 54–70% B; 7.1–13 min, 70–99%

B; 13–13.1 min, 99–40% B; 13.1–15 min, 40% B. The column temperature was 55 °C, the flow rate was 0.4 mL/min, and the injection volume was 5 μL.

The mass spectrometry conditions used were as follows: scan range, 70 ~ 1050 m/z; primary resolution, 70,000; automatic gain control, 3e6; maximum ion injection time, 100 ms; secondary resolution, 17,500; automatic gain control, 1e5; maximum ion injection time, 50 ms; and stepped normalized collision energy, 15, 30 and 45 eV. The electrospray ionisation (ESI) parameters were as follows: sheath gas flow rate, 40; Aux gas flow rate, 10; spray voltage (|KV|) in positive- and negative-ion mode, 3.80 and 3.20, respectively; capillary temperature, 320 °C; and aux gas heater temperature, 350 °C.

Lipid identification, differential lipid (DL) selection and functional enrichment analysis

Lipidsearch v.4.1 (Thermo Fisher, USA) was used for peak extraction and identification from off-line mass spectrometry data. After filtering and filling, the data were normalized to obtain relative peak areas using probabilistic quotient normalization. The identified lipids were classified and subjected to functional annotation analysis via the KEGG Compound database and Human Metabolome Database (HMDB, https://hmdb.ca/). Supervised partial least squares-discriminant analysis (PLS-DA) and orthogonal partial least squares-discriminant analysis (OPLS-DA) were used to detect significant differences in lipid abundance between LTF and HTF. The following thresholds were used to identify DLs: variable important for the project (VIP) value of OPLS-DA ≥ 1, FC ≥ 1.2 or ≤ 0.83 and *P* value < 0.05. Annotated DLs were first mapped to the KEGG pathway database. Pathways with *P* value < 0.05 according to a minimum hypergeometric test were identified as significantly enriched pathways. The metabolites identified were also submitted to MetaboAnalyst platform for pathway enrichment analysis.

HM400-targeted metabolome profiles of tail adipose tissue

The LC–MS QTRAP 6500+ (SCIEX) platform (BGI) was used to analyze 12 adipose tissue samples. HM400 mixed standard was serially diluted to prepare a standard curve. An appropriate amounts of sample and quality control sample were homogenized in 140 μL of 50% methanol water solution and centrifuged to obtain the supernatant. After the derivatization reaction, the mixtures were diluted with HM400 diluent and centrifuged at 12,000 rpm at 4 °C for 10 min. The supernatant was collected for LC–MS/MS analysis. The liquid chromatographic parameters were as follows: column, BEH C18 (1.7 μm, 2.1 mm×100 mm, Waters). The mass spectrometry parameters used were as follows: ion source, ESI+/ESI-. HMQuant software (BGI) was used for the automatic identification and integration of each multiple reaction monitoring transition. The content of each substance in HM400 (μmol/g) = C*A/m; C is the concentration value obtained using the standard curve (μmol/L) and the integrated peak area of the target index in the sample; A is the dilution factor, 0.14-; and m is the mass of the weighed solid sample (mg).

The metabolites were submitted to the KEGG database and HMDB for functional annotation. Additionally, PLS-DA was performed. Combining ratio analysis and t tests, the metabolites with ratios ≥ 1.2 or ≤ 0.83 and *P* values < 0.05 were defined as DMs. Spearman correlation analysis between DMs was performed using the R package corr. A *P* value < 0.05 was considered to indicate statistical significance. Pathway enrichment analysis of the DMs was conducted using the KEGG database and MetaboAnalyst.

Results

Transcriptome profiling of tail adipose tissue

Overview of transcriptome

A total of 178.15 and 180.61 million clean reads were obtained from LTF and HTF, respectively. Q30% ranged from 88.12 to 92.39%. A total of 86.16–87.89% of the clean reads were mapped successfully to the reference genome, and 67.31–79.67% of the clean reads presented unique hits, and 54.27–58.35% of the clean reads were mapped to the gene set using Bowtie 2 (Table S2).

Differential expression mRNAs in LTF and HTF

A total of 33,603 mRNAs and 17,178 genes were identified in LTF and HTF. A total of 16,483 and 16,720 genes were identified in LTF and HTF, respectively. In the comparison between LTF and HTF, the expression levels of 73 genes were significantly upregulated (upregulated DEGs) and those of 110 genes were significantly downregulated (downregulated DEGs) in LTF according to the default threshold (Fig. 2A, Table S3). The number of DEGs is not as high as in other similar studies [8, 9], which may be related to the same feeding environment and feed. A heatmap and boxplot were generated to show the expression patterns of the DEGs (Fig. 2B, C). There were more genes with higher expression levels in HTF than in LTF. There were 18 DEGs with GO terms related to lipid metabolism, such as *UCP3*, *PLCD3* and *ELOVL7* (Table S4). Some other DEGs, such as *CD5L*, *GSTA1*, *PPP3R1A*, *MEOX2*, *ADRA1D* and *FLT1*, reportedly participate in lipid metabolism according to records in the UniProt database but were not annotated to GO terms related to lipid metabolism.

Functional annotation of DEGs

The significantly enriched GO terms for biological processes, cellular components and molecular functions are presented in Fig. 2D and Table S5. Among the

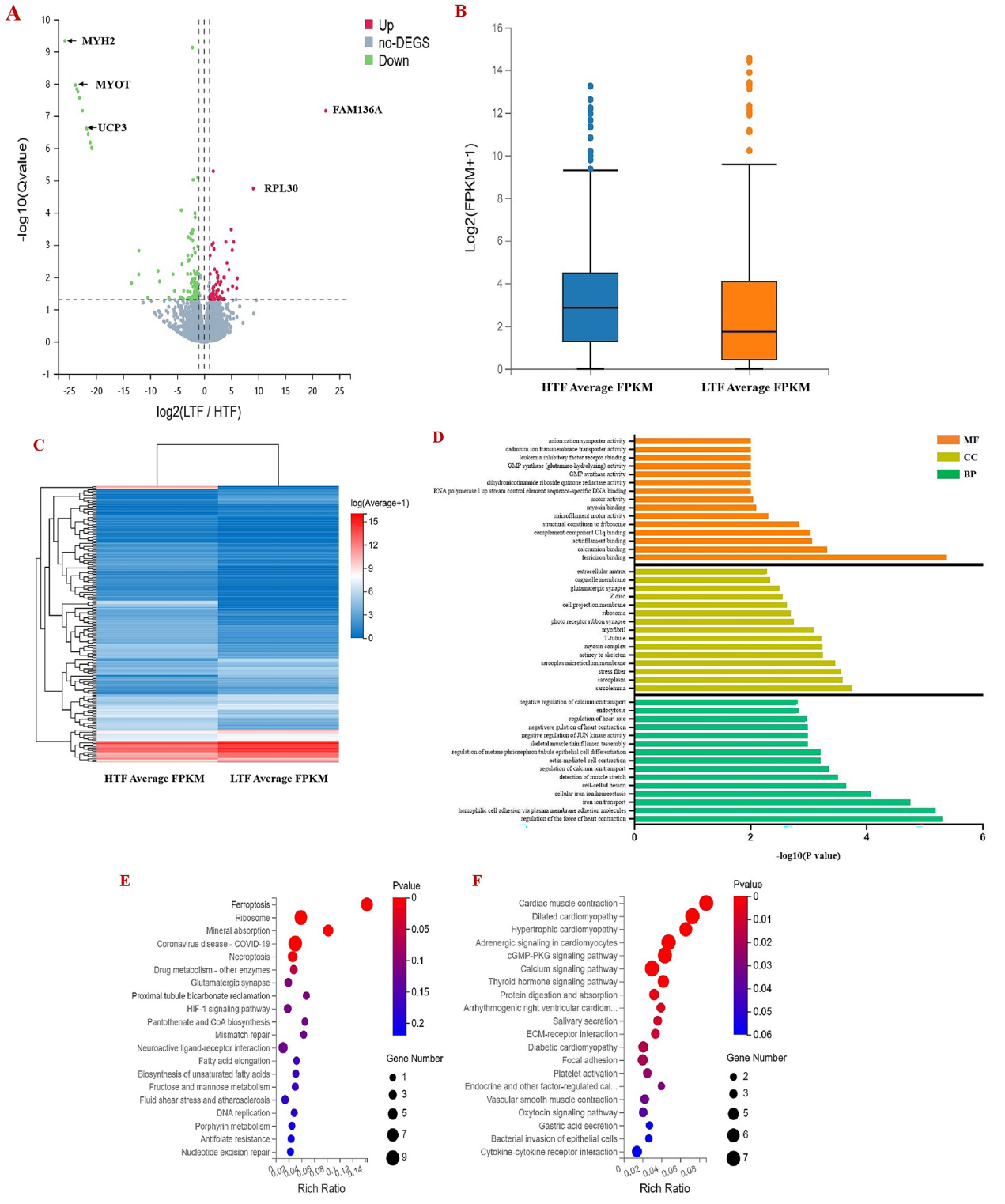

Fig. 2 Gene expression patterns of DEGs in the comparison between LTF and HTF. **A**, Volcanic map of DEGs. B, The boxplot of the expression of DEGs. **C**, The heat map of DEGs. **D**, The top 15 enriched Gene Ontology terms of molecular function (MF), cellular components (CC) and biological process (BP) with DEGs. **E**, The top 20 significantly enriched KEGG pathways with upregulated DEGs. **F**, The top 20 enriched KEGG pathways with downregulated DEGs. **G**, The protein-protein interaction network of proteins encoded by DEGs

significantly enriched GO terms, "cell adhesion" was the biological process category with the largest number of DEGs, containing 9 DEGs. The term "ribosome" was the most enriched cellular components term, containing 8 upregulated DEGs, and "calcium ion binding", enriched with 15 DEGs, was the most enriched molecular function term. Ribosome is the most enriched cellular components term, which may indicate that there is more active translation in LTF than in HTF. The upregulated DEGs were enriched mainly in the GO terms related to metal ion homeostasis and transmembrane transport (e.g., *FTL*, *FTH1* and *SLC39A8*), heme metabolic processes (e.g., *HMOX1* and *DTNBP1*), the inflammatory response (e.g., *JAGN1*, *PTX3* and *LGALS3*), fatty acid elongation (*ELOVL7*), amino acid and oligopeptide transport (*SLC38A3* and *LOC101111847*), G protein-coupled receptor signaling (*GMPS*, *VIPR1* and *ITPKA*), phagocytosis (e.g., *TREM2*, *LGALS3* and *HERPUD1)* and ribosome (e.g., *RPL38*, *RPS27* and *RPL36*). The downregulated DEGs were enriched mainly in the GO terms related to calcium ion transport (*CAV3*, *PLN* and *HRC*), the actin cytoskeleton (e.g., *ACTC1*, *RND1* and *CAV3*), the negative regulation of JUN kinase activity (e.g., *SFRP2* and *DUSP10*), the regulation of NIK/NF-kappaB signaling (e.g., *NOL3* and *BCL3*), the positive regulation of Rho protein signal transduction (e.g., *COL3A1* and *ABRA*), cell adhesion (e.g., *CD93*, *CDH11* and *CDH19*), endocytosis (e.g., *CAV3*, *DNM1* and *ENPP2*), the extracellular matrix (e.g., *COL3A1*, *OLFML2B* and *COL6A6*), and the glutamatergic synapse (e.g., *STXBP1*, *CLSTN3* and *CDH11*).

KEGG enrichment analysis revealed the top twenty pathways enriched with upregulated and downregulated DEGs in LTF and HTF (Fig. 2E, F and Table S6). As shown in Fig. 2E and F, the upregulated DEGs were significantly enriched in KEGG pathways such as ferroptosis (e.g., *FTL*, *LOC101105484* and *SAT1*) and mineral absorption (e.g., *FTH1*, *HMOX1* and *FTL*). Among the downregulated DEGs, fifteen genes (e.g., *PLN*, *ADRA1D* and *MYLK2*) were enriched in KEGG pathways related to the circulatory system and cardiovascular disease. Eleven downregulated DEGs (e.g., *HRC*, *MYH7* and *GUCY1A3*) were enriched in the calcium signaling pathway and cGMP-PKG signaling pathway. Several genes were enriched in ECM-receptor interactions (e.g., *COL6A6*, *COL6A3* and *FREM1*). A protein–protein interaction network was next generated using STRING. The network included 177 protein–protein nodes (Fig. 2G), and the essential core nodes of the network were ATP2A1, TTN, ACTA1, MYH1, RPL38, RPS29, FTH1, ISG15, CAV3 and COL3A1.

The expression of six DEGs in the tail adipose tissues of LTH and Hu sheep was quantified via RT–qPCR (Fig. S1). The RT–qPCR results confirmed the accuracy of the RNA-seq data.

Lipidomic profile of tail adipose tissue

Overall lipid composition characteristics

Using UPLC-MS, 345 lipids in five classes, including fatty acids (FAs, 2), glycerolipids (GLs, 57), saccharolipids (SLs, 1), glycerophospholipids (GPs, 250), and sphingolipids (SPs, 35), were identified in the 12 tail adipose tissue samples from LTH and Hu sheep (Fig. 3A, Table S7). The identification of detailed lipid components of tail fat is useful for further studies on the utilization of tail fat in sheep. The 345 lipids were submitted to the KEGG and HMDB databases for annotation, but only 11 lipids were annotated successfully. The contents of different types of lipids in LTF and HTF were compared and were listed in Fig. 3B and C. The contents of glycerolipids and glycerophospholipids in LTF were greater than those in HTF. Specifically, the contents of diglyceride (DG), triglyceride (TG), phosphatidylcholine (PC), dimethylphosphatidylethanolamine (dMePE), lysophosphatidylethanolamine (LPE), phosphatidylglycerol (PG), lysophosphatidylinositol (LPI), phosphatidic acid (PA), phosphatidylethanolamine (PE) and phosphatidylinositol (PI) were greater in LTF, and the contents of ceramides (Cer), lysophosphatidylcholine (LPC), monogalactosyldiacylglycerol (MGDG), phosphatidylethanol (PEt), phosphatidylserine (PS) and sphingomyelin (SM) were greater in HTF.

Differential lipids in tail adipose tissues of LTF and HTF and correlation analysis

The PLS-DA and OPLS-DA results for LTF and HTF are presented in Fig. 3D and E. Using the aforementioned thresholds for identifying significant differences in lipid abundance, we identified 55 DLs, including 27 increased and 28 decreased lipid metabolites (Fig. 3F, Table S8); a heatmap of DLs is presented in Fig. 3G.

The Spearman correlation coefficient between the first 20 DLs with the smallest *P* value was calculated to analyze the correlation between each DL. As shown in Fig. 3H, there was a strong positive correlation between the levels of phosphatidylcholines, such as PC (18:0/22:4) and PC (40:4) (0.993), PC (18:0/18:1) and PC (36:1) (0.986). PCs were strongly correlated with other kinds of lipids, such as PC (31:0) and PI (16:0/18:1) (0.951), PC (31:0) and LPI (16:0) (0.909). Triglycerides, TG (15:1/16:0/18:1), were negatively correlated with most other lipids, except for a positive correlation with PC (29:0) (0.594). The correlation network for the top 20 DLs with the smallest *P* value is presented in Fig. 3I, and the network had 19 nodes, without TG (15:1/16:0/18:1).

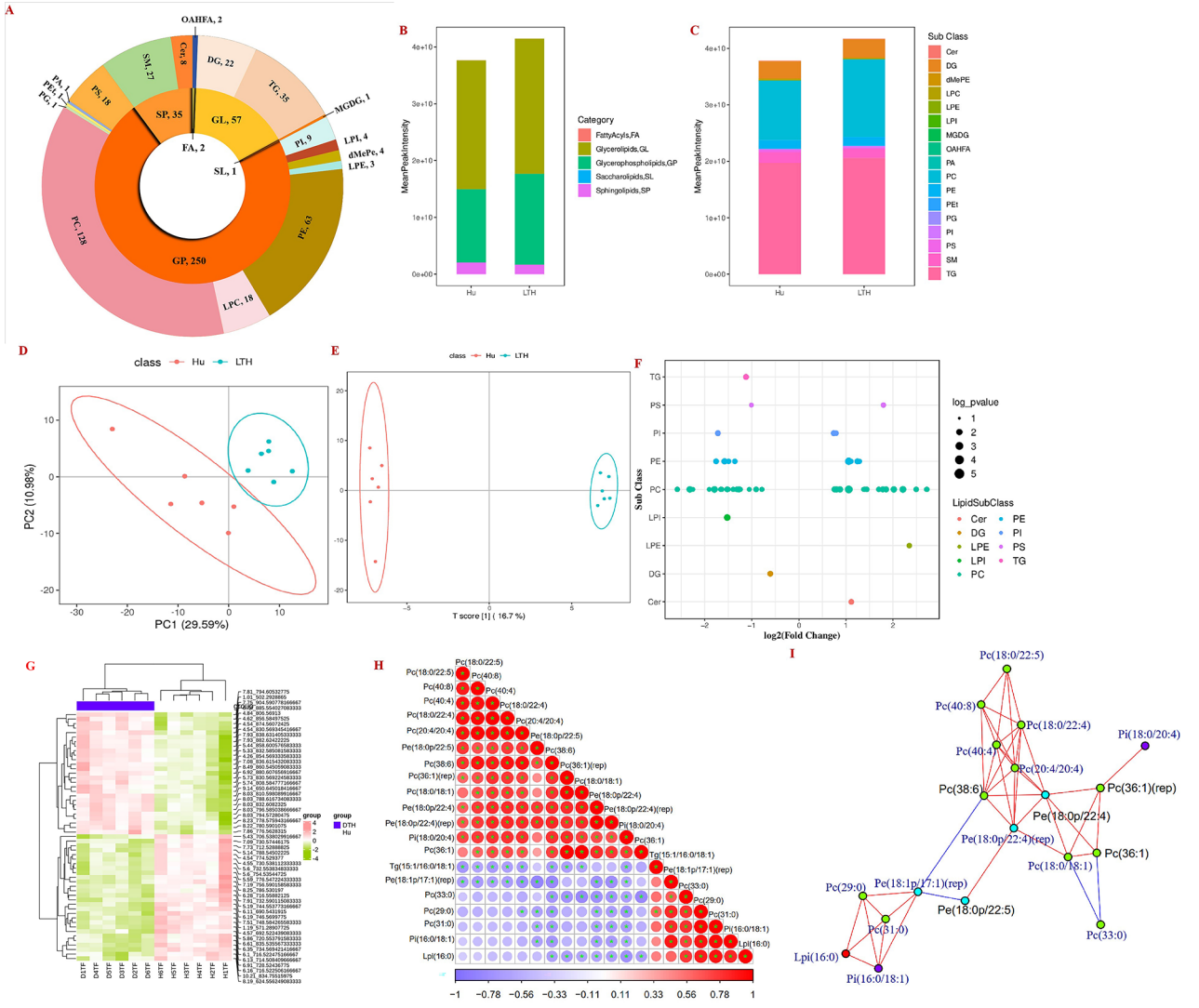

Fig. 3 Difference in lipid composition of tail adipose tissue between LTH and Hu sheep. **A**, Pie charts of lipids detected in LTF and HTF. **B** and **C**, The contents of different types of lipids. **D**, The supervised partial least squares-discriminant analysis (PLS-DA). **E**, The orthogonal partial least squares-discriminant analysis (OPLS-DA). **F**, The bubble diagram of DLs. **G**, The heatmap of DLs. **H**, The correlation between the top 20 DLs with the smallest *P*-value. **I**, The correlation network of the top 20 DLs with the smallest *P* value

Functional enrichment of differential lipids

The 55 DLs were submitted to the MetaboAnalyst online platform and KEGG database to perform lipidomic pathway analysis. There were eight significantly enriched pathways (Table S9). In the MetaboAnalyst database, "oligodendrocyte specification and differentiation" and "immunoregulatory interactions between lymphoid and nonlymphoid cells" were the most significantly enriched pathways. Only one pathway, "ferroptosis", was enriched significantly in the KEGG database. Notably, in the DEGs analysis, the ferroptosis pathway was also shown to be enriched (Table S5), which provided new ideas for the mechanisms of the dynamic changes of tail fat deposition in long fat-tailed sheep.

Targeted metabolomic analysis of tail adipose tissue

Using HM400-targeted quantification of 400 metabolites, 203 metabolites were detected in the tail adipose tissue of LTH and Hu sheep; the classification of the 203 metabolites is presented in Fig. 4A. PLS-DA was used to detect significant differences between LTF and HTF in the absolute quantitative results for metabolites (Fig. 4B). Seventeen DMs, including 8 increased and 9 decreased metabolites, were identified (Fig. 4C, Table S10). The DMs (Fig. 4D) with strong positive correlations were acetylglycine and 7-dehydrocholic acid (0.839), acetylglycine and N-acetyl-L-aspartic acid (0.953), adenosine monophosphate (AMP) and cis-aconitic acid (0.975), AMP and citric acid (0.972), cis-aconitic acid and citric acid (0.999), isovalerylglycine and L-lactic acid (0.918),

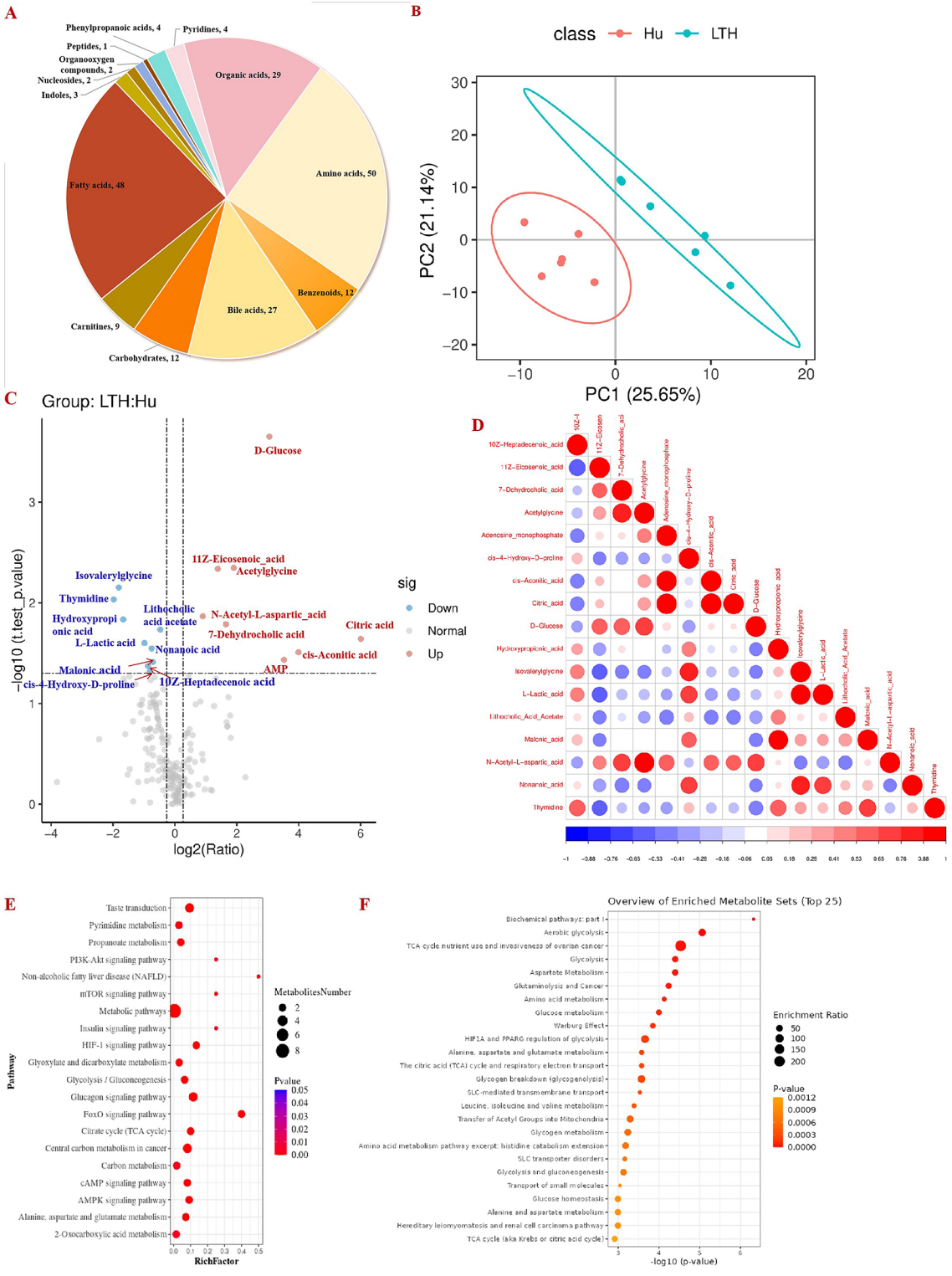

Fig. 4 Metabolism profile of LTF and HTF. **A**, the Pie charts of 203 metabolites detected in LTF and HTF. **B**, PLS-DA. **C**, Volcanic map of DMs. **D**, The correlation between DMs. **E** and **F**, Signaling pathways of DMs enriched in KEGG database and MetaboAnalyst database, respectively

isovalerylglycine and nonanoic acid (0.810), and hydroxypropionic acid and malonic acid (0.912). The correlations between 11Z-eicosenoic acid and 10Z-heptadecenoic acid (-0.647), and between 11Z-eicosenoic acid and isovalerylglycine (-0.563) were moderately negative.

DMs enrichment was analyzed using the KEGG database, and 45 pathways were significantly enriched (Table S11), and the top 20 pathways are presented in Fig. 4E. The most significantly enriched pathways were the "glucagon signaling pathway (citric acid, D-glucose and L-lactic acid)", "taste transduction (AMP, citric acid and D-glucose)" and "central carbon metabolism in cancer (citric acid, D-glucose and L-lactic acid)". The terms "cGMP-PKG signaling pathway" and "mineral absorption" were also enriched in the DEG analysis. Additionally, the DMs were submitted to the MetaboAnalyst online platform; the top 25 enriched pathways are presented in Fig. 4F.

Discussion

As an important organ for energy reservoirs in fat-tailed sheep, adipose tissue plays a critical role in surviving and thriving in extreme environments. To understand the mechanisms associated with long fat-tail development and identify useful lipids for the utilization of germplasm resources, we compared the transcriptome, lipidome and metabolome of adipose tissues in the tails of LTH and Hu sheep.

In this study, several genes and signaling pathways were found to be associated with fat deposition. Elongation of very long-chain fatty acid (ELOVL) proteins play critical roles in the regulation of the elongation of long-chain fatty acids. *ELOVL7* specifically elongates very long-chain CoA lipids (C17-C25 acyl-CoAs) [23]. Parisi et al. reported that the overexpression of *ELOVL7* causes the accumulation of very-long-chain fatty acids (VLCFAs) and increased permeability of the plasma membrane and that suppression of *ELOVL7* activity depletes the levels of VLCFAs that specifically accumulate during necroptosis and prevents membrane permeabilization and increases cell viability during necroptosis [24]. In LTF, *ELOVL7* was an upregulated DEG, and another DEG, *SLC27A6*, encoding long-chain fatty acid transport protein 6, an important transport protein for the synthesis of long-chain fatty acids, was also upregulated in LTF. *ELOVL7* increases the levels of phospholipids such as phosphatidylcholines [24]. Among the 55 DLs (Table S8), 36 DLs were phosphatidylcholines, with 17 increased and 19 decreased. Another DEG, *DEGS1*, also known as *FADS7*, encodes delta 4-desaturase, sphingolipid 1, which belongs to the fatty acid desaturase family and acts as a rate-limiting enzyme responsible for the desaturation of long-chain polyunsaturated fatty acids (PUFAs) during PUFA synthesis [25]. In LTF, the expression of both *ELOVL7* and *DEGS1* was upregulated, and the expression of several genes (e.g., *FTL* and *FTH1*) related to necroptosis and ferroptosis was also upregulated. The correlation or crosstalk among the elongation of VLCFAs, the desaturation of long-chain PUFAs, necroptosis and ferroptosis pathway in adipose tissues of sheep tail is not yet clear. The fatty acid composition and the amount of saturated/unsaturated fatty acids in phospholipids can affect cell membrane fluidity, which can be influenced by temperature [26]. In C2C12 cells, the synthesis of very long-chain saturated fatty acids and the expression of *ELOVL7* are promoted by mild and severe heat stress [26]. In LTF, among the 36 differential PCs, the 17 increased PCs were monounsaturated or polyunsaturated VLCFAs or branched long-chain fatty acids and among the 19 decreased PCs, 7 PCs were very long-chain saturated fatty acids (C29-C33). In LTF, even though the expression of *ELOVL7* was greater than that in HTF, the content of very-long-chain saturated fatty acids was lower, and the content of very-long-chain unsaturated fatty acids was greater than those in HTF, effects that may be related to the desaturation of long-chain PUFAs by the DEGS1 protein. These results may suggest that the cell membrane fluidity of HTF is easily affected by higher temperatures and that LTF has a more stable cell membrane; however, these findings requires experimental verification. *ELOVL7* and *DEGS1* are vital candidate genes for understanding the mechanism of tail fat deposition in sheep and would be investigated in the further studies.

The ferroptosis pathway, which is related to lipid metabolism, was enriched in the DEGs and DLs. Ferroptosis is driven by iron-dependent phospholipid (PL) peroxidation [27]. The unique signature of ferroptosis is the formation and accumulation of lipid hydroperoxides, particularly oxidized forms of polyunsaturated PEs, which act as death signals and drive cell death [28]. In LTF, the contents of six PEs (PE (18:0p/22:5), PE (18:0/22:4), PE (18:0p/22:4), PE (18:0p/22:4), LPE (20:4) and PE (40:4)) were greater than those in HTF, and in HTF, the contents of four PEs (PE (16:1/18:1), PE (17:1/18:1), PE (18:1p/17:1)(rep), and PE (34:2)) were lower than those in LTF. Among them, PE (18:0/22:4) was found to be a biomarker of ferroptosis [29, 30]. In animal cells, lactic acid can be oxidized by lactate oxidase to generate hydrogen peroxide, which participates in the Fenton reaction, and the latter enhances reactive oxygen species generation and ferroptosis [31]. The content of L-lactic acid was lower in LTF than in HTF. High glucose facilitates glycolysis and pyruvate oxidation, and stimulates citrate-mediated fatty acid synthesis, which ultimately promotes lipid peroxidation-dependent ferroptosis in multiple cell types [32–34]. The contents of glucose and citric acid were greater in LTF than in HTF (Table S10). The higher expression of genes related to ferroptosis (e.g., *FTL*,

SLC39A8 and *SAT1*, Table S6), higher content of glucose and citric acid, and lower content of lactate in LTF may suggest that the ferroptosis pathway was more active in LTF than in HTF.

Xu et al. reported that the tail adipose tissue of fat-tailed sheep has more stable ECM regulation than that of thin-tailed sheep [8]. In this study, the ECM-receptor interaction pathway was significantly enriched (Table S6). ECM-receptor interactions constitute one of the classical pathways of fat metabolism and strongly affect the functions of adipocytes [12]. ECM remodeling contributes to changes in adipocyte size and number [8, 35]. The ECM receptor interaction pathway was also shown to been enriched in other studies on the gene expression profiling of tail adipose tissue of sheep [36, 37]. The expression of DEGs related to ECM receptor interaction and focal adhesion, which are related to adipocyte size and morphology [38], such as *COL6A6*, *COL6A3*, *FREM1*, *CAV3* and *MYLK2*, was lower in LTF than in HTF. Long fat-tailed sheep may have less demand to regulate the size and shape of adipocytes and the extracellular environment in summer because of their well-maintained adipose tissue homeostasis [8].

The uncoupling protein 3 (*UCP3*) gene, a deregulated DEG ($\log_2$(FC)= -21.46) in LTF, encodes the putative mitochondrial transporter UCP3, a member of the mitochondrial carrier protein superfamily SLC25, and is expressed mainly in brown adipose tissue, muscles, and the heart [39]. *UCP3* induces fatty acid oxidation, promotes glucose uptake/utilization and decreases triglyceride and diglyceride storage in sarcoplasm/mitochondria [40]. However, the content of D-glucose in LTF was significantly greater than that in HTF, and the contents of TG (15:1/16:0/18:1) and DG (17:1/18:1) in LTF were lower than those in HTF, and the contents of 22 DGs and 34 other TGs were not significantly different between LTF and HTF. These findings may indicate different interactions among UCP3, glucose and TG (15:1/16:0/18:1)/DG (17:1/18:1) in the tail adipose tissue of sheep. *UCP3* also regulates the beta-adrenergic receptor signaling pathway to modulate pig adipocyte browning [41]. In this study, adrenergic signaling in cardiomyocytes was significantly enriched (Table S6). Wang et al. reported that folic acid supplementation downregulated the expression of *UCP3* in muscle [42], and in this study, the expression of one DEG, *FOLR3*, which encodes folate receptor gamma, was upregulated in LTF. However, whether there is a functional relationship between *FOLR3* and *UCP3* in the tail adipose tissue in sheep remains unclear. The expression of *UCP3* was significantly lower in LTF than in HTF, and the expression level of the other two UCP genes, *UCP1* and *UCP2* were not significantly different between LTF and HTF. The function of *UCP3* in the tail adipose tissue in sheep should be addressed in future studies. UCP3 is a molecular determinant of the effects of thyroid hormones on energy metabolism and heat production [39]. Thyroid hormones (THs), crucial hormones in lipid metabolism, regulate the expression of genes that play crucial roles in lipid metabolism, thermogenesis and nutrient availability [43]. Thyroid hormones regulate mitochondrial biogenesis and mTOR-mediated mitophagy to activate brown adipose tissue and induce the expression of uncoupling proteins to induce uncoupled respiration and heat production [44]. The lower expression levels of DEGs related to the thyroid hormone signaling pathway (*PLN*, *ATP2A1*, *PLCD3*, *ATP1A2* and *MYH7*) in LTF may suggest that lipolysis is not as active in LTF as it is in HTF. In addition, the thyroid hormone signaling pathway regulates adipocyte differentiation and adipogenesis [43, 45]. The expression patterns of DEGs related to the thyroid hormone signaling pathway in LTF also support less demand for reshaping adipocytes in LTH sheep, a finding that is consistent with the expression patterns of DEGs related to focal adhesion and ECM-receptor interactions. Leukemia inhibitory factor may be a marker of the differentiation of mesenchymal cells into adipocytes [46]. The downregulated expression of the leukemia inhibitory factor (*LIF*) gene in LTF is also evidence supporting the above viewpoint.

PPP1R3A encodes the glycogen-targeting subunit (G_M/R_{GL}) of protein phosphatase 1. Homozygous $G_M^{-/-}$ mice show impaired glucose tolerance and massive abdominal and heart fat deposition because of impaired blood glucose utilization in skeletal muscle [47]. Sánchez-Pozos et al. reported that a SNP (rs1799999) in *PPP1R3A* is associated with type 2 diabetes and that individuals with AC/AA genotypes present higher triglyceride and low-density lipoprotein levels, and lower concentrations of high-density lipoprotein [48]. *PPP1R3A*-modulated lipid metabolism may be associated with glycogen utilization, and the lower expression of *PPP1R3A* tends to be associated with a decrease in glycogen storage in tissues. In this study, the expression of *PPP1R3A* was significantly lower in LTF ($\log_2$(FC)= -23.057) than in HTF, and the contents of D-glucose, citric acid and cis-aconitic acid related to the tricarboxylic acid cycle were greater in LTF than in HTF. Whether lower expression of *PPP1R3A* promotes more glycogen utilization through the tricarboxylic acid cycle in the tail fat of sheep needs to be investigated further. Growth differentiation factor 10 (GDF10), which belongs to the transforming growth factor beta superfamily, is a novel regulator of adipogenesis. Yousof et al. reported a negative correlation between plasma GDF10 levels and body mass index, low-density lipoprotein-cholesterol, and total cholesterol levels in children aged 5–17 years [49]. However, Song et al. reported a positive correlation between the serum GDF10 concentration and body mass index in adult men [50]. The expression of

human *GDF10* is significantly lower in visceral fat than in subcutaneous fat [50]. In LTH sheep, the mRNA abundance of *GDF10* was not significantly different between perirenal fat and subcutaneous fat, and the mRNA abundance in tail fat was significantly lower than that in perirenal fat (unpublished data). In mice, GDF10 can block de novo lipogenesis to protect against endoplasmic reticulum stress by attenuating nuclear peroxisome proliferator-activated receptor gamma (PPARgamma, encoded by the *PPARG* gene) [51], and in LTH sheep, the mRNA abundance of *PPARG* did not significantly differ among tail fat, perirenal fat and subcutaneous fat (unpublished data).

The cGMP-PKG signaling pathway, one pathway significantly enriched with DEGs, mediates the regulation of the contraction and relaxation of vascular smooth muscle cells [52]. The vascular smooth muscle cells in the tail fat of sheep with different tail types may display different contraction and relaxation patterns, leading to different blood volumes, and subsequently to differences in the delivery of glucose, triglyceride and fatty acid to adipocytes and differences in adipogenesis and lipolysis in the tail fat. Additionally, the regulatory role of some signals, such as cardiac β3-adrenoceptors [53], nitric oxide [54], and natriuretic peptide [55, 56], in adipocyte differentiation and lipid metabolism occurs through the cGMP-PKG pathway. The storage and release of calcium are also regulated by the cGMP-PKG pathway in adipocytes. Increased intracellular Ca^{2+} stimulates the expression of lipogenic genes, such as *FAS*, to control de novo lipogenesis and promote triglyceride accumulation and lipid storage [57, 58]. Ca^{2+} also seems to regulate the thermogenic action of brown adipocytes [58]. The resting cytosolic calcium content is maintained by Sarco/endoplasmic reticulum calcium ATPase (SERCA) [58]. In brown adipocytes, the full potentiation of sarcoplasmic reticulum (SR)-calcium release requires alpha-adrenergic receptors and the phospholipase C-dependent opening of inositol triphosphate receptors on the SR membrane [59]. In this study, the calcium signaling pathway, which included 7 downregulated DEGs and 1 upregulated DEG, was a significantly enriched signaling pathway. Some DEGs have been reported to be associated with adipocytes and lipid metabolism. *ATP2A1* encodes SERCA1, which maintains the resting cytosolic calcium content of cells in adipose tissue [58] and is also a critical modulator of the obesity phenotype in humans [60]. The *PLN* encodes phospholamban, the first identified member of the regulin family, which is a family of small transmembrane proteins that modulate SERCA activity [61]. *ADRA1D* encodes adrenoceptor alpha 1D, an alpha-1-adrenergic receptor, and *PLCD3* encodes phospholipase C delta 3. Adrenoceptor alpha 1D and phospholipase C delta 3 are necessary for SR-calcium release in brown adipocytes [59].

Obesity and multiple obesity-associated diseases, including type 2 diabetes and cardiovascular disease, are increasing worldwide [62]. Excess central fat accumulation causes metabolic disturbance and increases the risk of diabetes mellitus and cardiovascular diseases [63, 64]. Obesity in mice causes defects in myocardial glucose metabolism, which leads to ventricular hypertrophy and cardiac dysfunction [65]. Fat deposited around the waist of males increases the risk of metabolic disorders, whereas fat deposited around the hips of females does not increase the risk of metabolic disorders, and may have some benefits [63, 64]. Therefore, it is important to determine which parts of fat deposits are the key factors of metabolic diseases. Fat deposited in the tail reduces fat distribution in other body parts of LTH sheep and can protect the heart and other organs. The expression levels of genes related to cardiomyopathy, platelet activation and vascular smooth muscle contraction, such as *PLN*, *LMNA* and *CACNG1*, were lower in LTF than in HTF. The expression of Cis-4-hydroxy-D-proline, a potential biomarker for the early diagnosis of acute myocardial infarction [66], was downregulated in LTH sheep. The acetylglycine content in serum is significantly negatively associated with the android fat/whole-body fat mass ratio, the android fat/gynoid fat mass ratio, and the whole-body fat percentage in humans [67–70]. In mice with high-fat diet-induced obesity, acetylglycine treatments reduce the weight of abdominal fat, subcutaneous fat, and visceral fat, and the fat/weight ratio [70]. Therefore, acetylglycine may affect fat distribution in body parts. Acetylglycine also modulates the expression of genes related to obesity-associated pathways in multiple types of adipose tissue [71]. Whether acetylglycine affects fat deposition patterns in sheep with different tail types needs to be investigated. The large amount of fat deposited in the tails of LTH sheep may provide a useful model for research on the mechanisms of obesity, cardiovascular disease and fat deposition patterns.

Conclusion

Transcriptome, lipid and metabolite profiles of tail adipose tissue from long and short fat-tailed sheep populations in summer were generated. We found that *UCP3*, *ELOVL7*, *PPP1R3A*, and *GDF10* and several signaling pathways, e.g., ECM-receptor interactions, ferroptosis, the thyroid hormone signaling pathway and the calcium signaling pathway and tricarboxylic acid cycle contributed to the differences in lipid metabolism and the tail phenotype of sheep. The interaction relationship of *ELOVL7*, phosphatidylcholines biosynthesis, and ferroptosis signaling pathway was suggested for further study. The findings provided new insights into the mechanism of tail fat deposition of sheep with different phenotype.

Abbreviations

AMP	Adenosine monophosphate
BW	Body weight
DEG	Differentially expressed gene
DL	Differential lipid
DM	Differential metabolite
DG	Diglyceride
dscDNA	Double-stranded cDNA
ECM	Extracellular matrix
ELOVL	Elongation of very long-chain fatty acid
ESI	Electrospray ionisation
FC	Fold change
GO	Gene ontology
HMDB	Human metabolome database
HTF	Tail fat of Hu sheep
KEGG	Kyoto encyclopedia of genes and genomes
LC-MS/MS	Liquid chromatography tandem mass spectrometry
LPI	Lysophosphatidylinositol
LTF	Tail fat of Large-tailed Han sheep
LTH sheep	Large-tailed Han sheep
OPLS-DA	Orthogonal projections to latent structures discriminant analysis
PC	Phosphatidylcholine
PE	Phosphatidylethanolamine
PI	Phosphatidylinositol
PLS-DA	Partial least squares discriminant analysis
PUFA	Polyunsaturated fatty acid
RNA-seq	RNA-sequencing
RT–qPCR	Reverse transcription quantitative real-time PCR
SR	Sarcoplasmic reticulum
SERCA	Sarco/endoplasmic reticulum calcium ATPase
TG	Triglyceride
UCP	Uncoupling protein
UPLC-MS	Ultra performance liquid chromatography tandem mass spectrometry
VLCFA	Very long-chain fatty acid

Supplementary Information

The online version contains supplementary material available at https://doi.org/10.1186/s12864-025-11380-9 .

Supplementary Material 1

Supplementary Material 2

Supplementary Material 3

Acknowledgements
Not applicable.

Author contributions
G.C. and Y.J. designed the experiment and acquired funding; Y.J. and X.L.performed data analysis. Y.J. and H.L. collected the adipose tissues of tail. Y.J. and X.L. draft the article; M.C., Y.J. and X.L. reviewed and edited the paper.

Funding
This work was funded by Natural Science Foundation of Shandong Province, China (ZR2021MC130), Shandong Province Agricultural Seed Engineering Project (2019LZGC019), Open Project of Liaocheng University Animal Husbandry Discipline (31946220722), Key Research and Development plan in Liaocheng city (2022YDNY01).

Data availability
The sequencing data in this study can be found in the Sequence Read Archive under project number PRJNA1140355.

Declarations

Ethics approval and consent to participate
The animal study protocol was approved by the Animal Care and Use Committee of Liaocheng University (Shandong province, China) (Approval number: 2023042603, 26, April, 2023).

Consent for publication
Not applicable.

Competing interests
The authors declare no competing interests.

Author details
[1]School of Agriculture and Biology, Liaocheng University, Liaocheng 252059, China
[2]State Key Laboratory of Animal Biotech Breeding, Institute of Animal Science, Chinese Academy of Agricultural Sciences (CAAS), Beijing 100193, China
[3]Shandong Provincial Key Laboratory of Animal Biotechnology and Disease Control and Prevention, Shandong Agricultural University, Tai'an, China

Received: 26 July 2024 / Accepted: 18 February 2025
Published online: 03 March 2025

References

1. Kalds P, Luo Q, Sun K, Zhou S, Chen Y, Wang X. Trends towards revealing the genetic architecture of sheep tail patterning: promising genes and investigatory pathways. Anim Genet. 2021;52(6):799–812.
2. Rocha JL, Godinho R, Brito JC, Nielsen R. Life in deserts: the genetic basis of mammalian desert adaptation. Trends Ecol Evol. 2021;36:637–50.
3. Moradi MH, Nejati-Javaremi A, Moradi-Shahrbabak M, Dodds KG, Mcewan JC. Genomic scan of selective sweeps in thin and fat tail sheep breeds for identifying of candidate regions associated with fat deposition. BMC Genet. 2012;13:10.
4. Kridli RT, Said SI. Libido testing and the effect of exposing sexually Naive Awassi Rams to estrous Ewes on sexual performance. Small Ruminant Res. 1999;32:149–52.
5. Olschewsky A, Hinrichs D. An overview of the use of genotyping techniques for assessing genetic diversity in local farm animal breeds. Anim (Basel). 2021;11(7):2016.
6. Mishra AK, Ahlawat S, Sharma R, Arora R, Singh S, Jain A. Assessment of genetic diversity of the fat-tailed Dumba sheep of India by mitochondrial and microsatellite markers. Anim Biotechnol. 2023;34(8):3545–54.
7. Li X, Yang J, Shen M, Xie XL, Liu GJ, Xu YX, et al. Whole-genome resequencing of wild and domestic sheep identifies genes associated with morphological and agronomic traits. Nat Commun. 2020;11(1):2815.
8. Xu YX, Wang B, Jing JN, Ma R, Luo YH, Li X, et al. Whole-body adipose tissue multi-omic analyses in sheep reveal molecular mechanisms underlying local adaptation to extreme environments. Commun Biol. 2023;6(1):159.
9. Jin M, Fei X, Li T, Lu Z, Chu M, Di R, et al. Transcriptome study digs out BMP2 involved in adipogenesis in sheep Tails. BMC Genomics. 2022;23(1):457.
10. Bakhtiarizadeh MR, Salami SA. Identification and expression analysis of long noncoding RNAs in fat-tail of sheep breeds. (Bethesda). 2019;G3(4):1263–76.
11. Su XH, He HY, Fang C, Liu LL, Liu WJ. Transcriptome profiling of LncRNAs in sheep tail fat deposition. Anim Biotechnol. 2023;34(4):900–10.
12. Zhang Z, Zhang Y, Bao Q, Gu Y, Liang C, Chu M, et al. The landscape of accessible chromatin during Yak adipocyte differentiation. Int J Mol Sci. 2022;23(17):9960.
13. China National Commission of Animal Genetic Resources. Animal genetic resources in China: sheep and goats[M]. Beijing: China Agriculture; 2011. p. 67. (in Chinese).
14. Wang J, Zhang X, Wang X, Li F, Zhang D, Li X, et al. Polymorphism and expression of the HMGA1 gene and association with tail fat deposition in Hu sheep. Anim Biotechnol. 2023;34(4):1626–34.
15. Della Guardia L, Shin AC. Obesity-induced tissue alterations resist weight loss: A mechanistic review. Diabetes Obes Metab. 2024;26(8):3045–57.
16. Li R, Li Y, Kristiansen K, Wang J. SOAP: short oligonucleotide alignment program. Bioinformatics. 2008;24(5):713–4.

17. Kim D, Langmead B, Salzberg SL. HISAT: a fast spliced aligner with low memory requirements. Nat Methods. 2015;12:357–60.
18. Langmead B, Salzberg SL. Fast gapped-read alignment with bowtie 2. Nat Methods. 2012;9(4):357–9.
19. Li B, Dewey CN. RSEM: accurate transcript quantification from RNA-Seq data with or without a reference genome. BMC Bioinformatics. 2011;12:323.
20. Love MI, Huber W, Anders S. Moderated Estimation of fold change and dispersion for RNA-seq data with DESeq2. Genome Biol. 2014;15:550.
21. Yi C, Liu J, Deng W, Luo C, Qi J, Chen M, et al. Macrophage elastase (MMP12) critically contributes to the development of subretinal fibrosis. J Neuroinflammation. 2022;19(1):78.
22. Chang Jk, Li XP, Shen J, Hu J, Wu LF, Zhang XY, et al. Defects in the cell wall and its deposition caused by loss-of-function of three RLKs alter root hydrotropism in Arabidopsis thaliana. Nat Commun. 2024;15(1):2648.
23. Ferraz RB, Paixão RV, Lopes-Marques M, Machado AM, Salaro AL, Castro LFC, et al. The repertoire of the elongation of very long-chain fatty acids (Elovl) protein family is conserved in Tambaqui (Colossoma macropomum): gene expression profiles offer insights into the sexual differentiation process. Comp Biochem Physiol B Biochem Mol Biol. 2022;261:110749.
24. Parisi LR, Sowlati-Hashjin S, Berhane IA, Galster SL, Carter KA, Lovell JF, et al. Membrane disruption by very long chain fatty acids during necroptosis. ACS Chem Biol. 2019;14(10):2286–94.
25. Zhao T, Gao P, Li Y, Tian H, Ma D, Sun N, Chen C, Zhang Y, Qi X. Investigating the role of FADS family members in breast cancer based on bioinformatic analysis and experimental validation. Front Immunol. 2023;14:1074242.
26. Risha MA, Ali A, Siengdee P, Trakooljul N, Dannenberger D, Wimmers K, et al. Insights into molecular pathways and fatty acid membrane composition during the temperature stress response in the murine C2C12 cell model. Sci Total Environ. 2022;807(Pt 3):151019.
27. Liang D, Minikes AM, Jiang X. Ferroptosis at the intersection of lipid metabolism and cellular signaling. Mol Cell. 2022;82(12):2215–27.
28. Amoscato AA, Anthonymuthu T, Kapralov O, Sparvero LJ, Shrivastava IH, Mikulska-Ruminska K, et al. Formation of protein adducts with Hydroperoxy-PE electrophilic cleavage products during ferroptosis. Redox Biol. 2023;63:102758.
29. Du X, Ma X, Tan Y, Shao F, Li C, Zhao Y, et al. B cell-derived anti-beta 2 glycoprotein I antibody mediates hyperhomocysteinemia-aggravated hypertensive glomerular lesions by triggering ferroptosis. Signal Transduct Target Ther. 2023;8(1):103.
30. Tyurina YY, Kapralov AA, Tyurin VA, Shurin G, Amoscato AA, Rajasundaram D, et al. Redox phospholipidomics discovers pro-ferroptotic death signals in A375 melanoma cells in vitro and in vivo. Redox Biol. 2023;61:102650.
31. Zou W, Gao F, Meng Z, Cai X, Chen W, Zheng Y, et al. Lactic acid responsive sequential production of hydrogen peroxide and consumption of glutathione for enhanced ferroptosis tumor therapy. J Colloid Interface Sci. 2024;663:787–800.
32. Ma H, Wang X, Zhang W, Li H, Zhao W, Sun J, et al. Melatonin suppresses ferroptosis induced by high glucose via activation of the Nrf2/HO-1 signaling pathway in type 2 diabetic osteoporosis. Oxid Med Cell Longev. 2020;2020:9067610.
33. Song X, Liu J, Kuang F, Chen X, Zeh HJ, Kang R, et al. PDK4 dictates metabolic resistance to ferroptosis by suppressing pyruvate oxidation and fatty acid synthesis. Cell Rep. 2021;34(8):108767.
34. Yao X, Li W, Fang D, Xiao C, Wu X, Li M, et al. Emerging roles of energy metabolism in ferroptosis regulation of tumor cells. Adv Sci (Weinh). 2021;8(22):e2100997.
35. Ruiz-Ojeda FJ, Mendez-Gutierrez A, Aguilera CM, Plaza-Diaz J. Extracellular matrix remodeling of adipose tissue in obesity and metabolic diseases. Int J Mol Sci. 2019;20:4888.
36. Fei X, Jin M, Wang Y, Li T, Lu Z, Yuan Z, et al. Transcriptome reveals key MicroRNAs involved in fat deposition between different tail sheep breeds. PLoS ONE. 2022;17(3):e0264804.
37. Farhadi S, Hasanpur K, Ghias JS, Palangi V, Maggiolino A, Landi V. Comprehensive gene expression profiling analysis of adipose tissue in male individuals from fat- and thin-tailed sheep breeds. Anim (Basel). 2023;13(22):3475.
38. Xiong Y, Wang Y, Xu Q, Li A, Yue Y, Ma Y, et al. LKB1 regulates goat intramuscular adipogenesis through focal adhesion pathway. Front Physiol. 2021;12:755598.
39. Della Guardia L, Luzi L, Codella R. Muscle-UCP3 in the regulation of energy metabolism. Mitochondrion. 2024;76:101872.
40. Gentile A, Magnacca N, de Matteis R, Moreno M, Cioffi F, Giacco A, et al. Ablation of uncoupling protein 3 affects interrelated factors leading to lipolysis and insulin resistance in visceral white adipose tissue. FASEB J. 2022;36(5):e22325.
41. Kim S, Yazawa T, Koide A, Yoneda E, Aoki R, Okazaki T, et al. Potential role of pig UCP3 in modulating adipocyte Browning via the beta-adrenergic receptor signaling pathway. Biology (Basel). 2024;13(5):284.
42. Wang B, Li H, Li Z, Wang B, Zhang H, Zhang B, et al. Integrative network analysis revealed the molecular function of folic acid on immunological enhancement in a sheep model. Front Immunol. 2022;13:913854.
43. Obregon MJ. Adipose tissues and thyroid hormones. Front Physiol. 2014;5:479.
44. Yau WW, Singh BK, Lesmana R, Zhou J, Sinha RA, Wong KA, et al. Thyroid hormone (T(3)) stimulates brown adipose tissue activation via mitochondrial biogenesis and MTOR-mediated mitophagy. Autophagy. 2019;15(1):131–50.
45. Lee MJ. Hormonal regulation of adipogenesis. Compr Physiol. 2017;7(4):1151–95.
46. Falconi D, Oizumi K, Aubin JE. Leukemia inhibitory factor influences the fate choice of mesenchymal progenitor cells. Stem Cells. 2007;25:305–12.
47. Delibegovic M, Armstrong CG, Dobbie L, Watt PW, Smith AJ, Cohen PT. Disruption of the striated muscle glycogen targeting subunit PPP1R3A of protein phosphatase 1 leads to increased weight gain, fat deposition, and development of insulin resistance. Diabetes. 2003;52(3):596–604.
48. Sánchez-Pozos K, Ortíz-López MG, Peña-Espinoza BI, de Los Ángeles Granados-Silvestre M, Jiménez-Jacinto V, et al. Whole-exome sequencing in Maya Indigenous families: variant in PPP1R3A is associated with type 2 diabetes. Mol Genet Genomics. 2018;293(5):1205–16.
49. Yousof TR, Mejia-Benitez A, Morrison KM, Austin RC. Reduced plasma GDF10 levels are positively associated with cholesterol impairment and childhood obesity. Sci Rep. 2024;14(1):1805.
50. Song MK, Kim JE, Kim JT, Kang YE, Han SJ, Kim SH, et al. GDF10 is related to obesity as an adipokine derived from subcutaneous adipose tissue. Front Endocrinol (Lausanne). 2023;14:1159515.
51. Platko K, Lebeau PF, Byun JH, Poon SV, Day EA, MacDonald ME, et al. GDF10 blocks hepatic PPARgamma activation to protect against diet-induced liver injury. Mol Metab. 2019;27:62–74.
52. Xiong L, Pei J, Bao P, Wang X, Guo S, Cao M, et al. The effect of the feeding system on fat deposition in Yak subcutaneous fat. Int J Mol Sci. 2023;24(8):7381.
53. Arioglu-Inan E, Kayki-Mutlu G, Michel MC. Cardiac B3 -adrenoceptors-A role in human pathophysiology? Br J Pharmacol. 2019;176(14):2482–95.
54. Chen CW, Chen LK, Huang TY, Yang DM, Liu SY, Tsai PJ, Chen TH, Lin HF, Juan CC. Nitric oxide mobilizes intracellular Zn(2+) via the GC/cGMP/PKG signaling pathway and stimulates adipocyte differentiation. Int J Mol Sci. 2022;23(10):5488.
55. Liu D, Ceddia RP, Collins S. Cardiac natriuretic peptides promote adipose 'browning' through mTOR complex-1. Mol Metab. 2018;9:192–8.
56. Ai X, Hou X, Guo T. C-type natriuretic peptide promotes adipogenic differentiation of goat adipose-derived stem cells via cGMP/PKG/p38 MAPK signal pathway. Vitro Cell Dev Biol Anim. 2021;57(9):865–77.
57. Arruda AP, Hotamisligil GS. Calcium homeostasis and organelle function in the pathogenesis of obesity and diabetes. Cell Metab. 2015;22(3):381–97.
58. Guarnieri AR, Benson TW, Tranter M. Calcium cycling as a mediator of thermogenic metabolism in adipose tissue. Mol Pharmacol. 2022;102(1):51–9.
59. Leaver EV, Pappone PA. Beta-adrenergic potentiation of Endoplasmic reticulum $Ca^{(2+)}$ release in brown fat cells. Am J Physiol Cell Physiol. 2002;282(5):C1016–24.
60. Joslin AC, Sobreira DR, Hansen GT, Sakabe NJ, Aneas I, Montefiori LE, et al. A functional genomics pipeline identifies Pleiotropy and cross-tissue effects within obesity-associated GWAS loci. Nat Commun. 2021;12(1):5253.
61. Rathod N, Bak JJ, Primeau JO, Fisher ME, Espinoza-Fonseca LM, Lemieux MJ, et al. Nothing regular about the Regulins: distinct functional properties of SERCA transmembrane peptide regulatory subunits. Int J Mol Sci. 2021;22:8891.
62. Chinnasamy P, Casimiro I, Riascos-Bernal DF, Venkatesh S, Parikh D, Maira A, et al. Increased adipose catecholamine levels and protection from obesity with loss of allograft inflammatory Factor-1. Nat Commun. 2023;14(1):38.
63. Vasan SK, Osmond C, Canoy D, Christodoulides C, Neville MJ, Di Gravio C, et al. Comparison of regional fat measurements by dual-energy X-ray absorptiometry and conventional anthropometry and their association with markers of diabetes and cardiovascular disease risk. Int J Obes. 2018;42:850–7.
64. Marsh ML, Oliveira MN, Vieira-Potter VJ. Adipocyte metabolism and health after the menopause: the role of exercise. Nutrients. 2023;15(2):444.

65. Park SY, Cho YR, Finck BN, Kim HJ, Higashimori T, Hong EG, et al. Cardiac-specific overexpression of peroxisome proliferator-activated receptor-alpha causes insulin resistance in heart and liver. Diabetes. 2005;54:2514–24.
66. Zhou J, Hou HT, Song Y, Zhou XL, Chen HX, Zhang LL, et al. Metabolomics analysis identifies differential metabolites as biomarkers for acute myocardial infarction. Biomolecules. 2024;14(5):532.
67. Moore SC, Matthews CE, Sampson JN, Stolzenberg-Solomon RZ, Zheng W, Cai Q, et al. Human metabolic correlates of body mass index. Metabolomics. 2014;10:259–69.
68. Murphy RA, Moore SC, Playdon M, Meirelles O, Newman AB, Milijkovic I, et al. Metabolites associated with lean mass and adiposity in older black men. J Gerontol Biol Sci Med Sci. 2017;72(10):1352–9.
69. Cirulli ET, Guo L, Leon Swisher C, Shah N, Huang L, Napier LA, et al. Profound perturbation of the metabolome in obesity is associated with health risk. Cell Metab. 2019;29:488–e5002.
70. Su KJ, Chen XY, Gong R, Zhao Q, Hu SD, Feng MC, et al. Systematic metabolomic studies identified adult adiposity biomarkers with acetylglycine associated with fat loss in vivo. Front Mol Biosci. 2023a;10:1166333.
71. Fluhr L, Mor U, Kolodziejczyk AA, Dori-Bachash M, Leshem A, Itav S, et al. Gut microbiota modulates weight gain in mice after discontinued smoke exposure. Nature. 2021;600:713–9.

Publisher's note